New Journal of Physics
The open access journal at the forefront of physics

Deutsche Physikalische Gesellschaft DPG IOP Institute of Physics

Measurement of two-photon position–momentum Einstein–Podolsky–Rosen correlations through single-photon intensity measurements

To cite this article: Abhinandan Bhattacharjee *et al* 2022 *New J. Phys.* **24** 053033

New Journal of Physics
The open access journal at the forefront of physics

Deutsche Physikalische Gesellschaft DPG
IOP Institute of Physics

Published in partnership with: Deutsche Physikalische Gesellschaft and the Institute of Physics

OPEN ACCESS

RECEIVED
8 March 2021

REVISED
8 April 2022

ACCEPTED FOR PUBLICATION
21 April 2022

PUBLISHED
12 May 2022

PAPER

Measurement of two-photon position–momentum Einstein–Podolsky–Rosen correlations through single-photon intensity measurements

Abhinandan Bhattacharjee*, Nilakantha Meher and Anand K Jha*

Department of Physics, Indian Institute of Technology Kanpur, Kanpur, UP 208016, India
* Authors to whom any correspondence should be addressed.

E-mail: arko.hkd@gmail.com and akjha9@gmail.com

Keywords: quantum entanglement, EPR-correlation, spontaneous parametric down-conversion, interferometry

Supplementary material for this article is available online

Abstract

The measurement of the position–momentum Einstein–Podolsky–Rosen (EPR) correlations of a two-photon state is important for many quantum information applications ranging from quantum key distribution to coincidence imaging. However, all the existing techniques for measuring the position–momentum EPR correlations involve coincidence detection and thus suffer from issues that result in less accurate measurements. In this article, we propose and demonstrate an experimental scheme that does not require coincidence detection for measuring the EPR correlations. Our technique works for two-photon states that are pure, irrespective of whether the state is separable or entangled. We theoretically show that if the pure two-photon state satisfies a certain set of conditions then the position–momentum EPR correlations can be obtained by doing the intensity measurements on only one of the photons. We experimentally demonstrate this technique for pure two-photon states produced by type-I spontaneous parametric down-conversion, and to the best of our knowledge, we report the most accurate experimental measurement of position–momentum EPR correlations.

1. Introduction

If two photons are entangled in position and momentum variables, the product of the conditional position and momentum uncertainties of the individual photons becomes less than $0.5\hbar$, the minimum value allowed by the Heisenberg uncertainty relation. This violation of the conditional Heisenberg uncertainty relation is the signature of position–momentum Einstein–Podolsky–Rosen (EPR) correlations [1] and is a witness of the position–momentum entanglement. For two-dimensional variables, such as polarization, entanglement can be verified through the violations of Bell's inequalities [2] and can be quantified through measures such as concurrence [3]. However, for continuous variables, such as position–momentum, there is no prescription for quantifying entanglement. One can at best only verify entanglement, and the EPR-correlations measurements are the primary tools for that. In the past, several studies have used EPR-correlations measurements in the position–momentum variables in order to demonstrate position–momentum entanglement [4–11]. EPR-correlation measurements have also been used as witnesses of entanglement in many other continuous variables including time-energy [12–14], angle-orbital angular momentum (OAM) [15], radial position–radial momentum [16], and quadrature phase-amplitude [17]. More recently, even in entangled systems not consisting of photons, EPR-correlations measurements have become important tools for witnessing continuous-variable entanglement. These include macroscopic objects [18], Bose Einstein condensate [19], and cold atoms [20].

The demonstration of position–momentum EPR-correlations is very important for many applications such as quantum key distribution [21], quantum information processing [22], quantum metrology [23], quantum imaging [24–27], and quantum holography [28], since the efficiency of these applications relies

on how accurately the EPR correlations could be measured. Therefore, it is very important to have a more accurate technique for measuring EPR-correlations. In the past few years, many schemes with increased accuracy have been demonstrated [4–17]. However, all these methods involve coincidence detection, implemented either by using two scanning single-photon detectors [4], or two scanning slits [5, 6], or array of single-photon detectors [7, 8], or EMCCD cameras [9–11]. As a result, these measurement methods suffer from either too much loss of light, or strict alignment requirements, or multiple measurements, which adversely affect the accuracy of measurements.

On the other hand, in the context of two-dimensional two-particle state, that is, the two-qubit states, it is known that if the state is pure, the entanglement quantifiers [3, 29] can be measured by doing measurements on only one of the qubits [30, 31], without requiring coincidence detection. Furthermore, even in the context of continuous variables, it is known that when the two-photon state is pure, several two-photon properties such as two-photon angular Schmidt spectrum [32–34], two-photon spatial Schmidt number [35], and momentum correlations [36] can be measured by doing intensity measurements on only one of the photons. These measurement schemes based on intensity detection provide much better accuracy than those based on coincidence detection.

In this article, utilizing the same physics, we propose a technique for measuring the position–momentum EPR-correlations that does not require coincidence detection. Our technique is based on measuring the intensities of only one of the photons, and it works for two-photon states that are pure, irrespective of whether the state is separable or entangled. We show that if a pure two-photon state satisfies a certain set of conditions, the position–momentum EPR correlations can be obtained by doing the intensity measurements on only one of the photons. We experimentally demonstrate our technique with pure two-photon states produced by type-I spontaneous parametric down-conversion (SPDC), and we obtain, to the best of our knowledge, the most accurate measurement of position–momentum EPR-correlations reported so far.

2. Theory

A pure state of two photons $|\Psi\rangle$ in the transverse momentum basis can be written as

$$|\Psi| = \iint \mathrm{d}\boldsymbol{p}_1\, \mathrm{d}\boldsymbol{p}_2\, \psi(\boldsymbol{p}_1, \boldsymbol{p}_2)|\boldsymbol{p}_1, \boldsymbol{p}_2|. \tag{1}$$

Here, $\boldsymbol{p}_1 \equiv (p_{1x}, p_{1y})$ and $\boldsymbol{p}_2 \equiv (p_{2x}, p_{2y})$ are the transverse momenta of the first and the second photon, respectively, $|\boldsymbol{p}_1, \boldsymbol{p}_2\rangle$ is the two-photon state vector, and $\psi(\boldsymbol{p}_1, \boldsymbol{p}_2)$ represents the two-photon transverse-momentum wavefunction. We note that if the two-photon wavefunction satisfies $\psi(\boldsymbol{p}_1, \boldsymbol{p}_2) = \psi(\boldsymbol{p}_1)\psi(\boldsymbol{p}_2)$ then it is separable, otherwise it is non-separable, or in other words, entangled. When the second photon is detected with transverse momentum $\boldsymbol{p}_2 = 0$, then the conditional momentum probability distribution $P(\boldsymbol{p}_1|\boldsymbol{p}_2 = 0)$ of the first photon is given by

$$P(\boldsymbol{p}_1|\boldsymbol{p}_2 = 0) = |\psi(\boldsymbol{p}_1, \boldsymbol{p}_2 = 0)|^2. \tag{2}$$

The momentum cross-spectral density function of the first photon can be calculated as $W(\boldsymbol{p}_1, \boldsymbol{p}'_1) = \langle\Psi|E_1^{(+)}(\boldsymbol{p}_1)E_1^{(-)}(\boldsymbol{p}'_1)|\Psi\rangle$ [37], where $E_1^{(+)}(\boldsymbol{p}_1)$ and $E_1^{(-)}(\boldsymbol{p}'_1)$ are the negative- and positive-frequency parts of the electric field operator, respectively. For $\boldsymbol{p}'_1 = -\boldsymbol{p}_1$, we have

$$W(\boldsymbol{p}_1, -\boldsymbol{p}_1) = \iint \psi^*(\boldsymbol{p}_1, \boldsymbol{p}_2)\psi(-\boldsymbol{p}_1, \boldsymbol{p}_2)\mathrm{d}\boldsymbol{p}_2. \tag{3}$$

Next, we find that if the two-photon wavefunction satisfies the following condition

$$\psi^*(\boldsymbol{p}_1, \boldsymbol{p}_2)\psi(-\boldsymbol{p}_1, \boldsymbol{p}_2) \propto |\psi(\boldsymbol{p}_1, \boldsymbol{p}_2 = 0)\psi(\boldsymbol{p}_1 = 0, \boldsymbol{p}_2)|^2, \tag{4}$$

then using equations (2) and (3), one can show that

$$W(\boldsymbol{p}_1, -\boldsymbol{p}_1) \propto P(\boldsymbol{p}_1|\boldsymbol{p}_2 = 0). \tag{5}$$

We note that the condition in equation (4) can be satisfied by both separable and inseparable pure two-photon wavefunctions. Equation (5) is the main theoretical result of this article. It states that as long as a two-photon state is pure, whether separable or entangled, and satisfies the condition in equation (4), the momentum cross-spectral density function of the first photon remains proportional to its conditional momentum probability distribution function. This implies that the standard deviations of $W(\boldsymbol{p}_1, -\boldsymbol{p}_1)$ and $P(\boldsymbol{p}_1|\boldsymbol{p}_2 = 0)$ are equal and that by measuring the standard deviation of $W(\boldsymbol{p}_1, -\boldsymbol{p}_1)$, one can obtain the

standard deviation of $P(\boldsymbol{p}_1|\boldsymbol{p}_2 = 0)$. We denote the standard deviation of the conditional x-momentum of the first photon by $\Delta(p_{1x}|p_{2x} = 0)$.

By writing the two-photon wavefunction of equation (1) in the position basis and proceeding in the similar manner, we can show that if the two-photon position wavefunction $\psi(\boldsymbol{\rho}_1, \boldsymbol{\rho}_2)$ satisfies the condition

$$\psi^*(\boldsymbol{\rho}_1, \boldsymbol{\rho}_2)\psi(-\boldsymbol{\rho}_1, \boldsymbol{\rho}_2) \propto |\psi(\boldsymbol{\rho}_1, \boldsymbol{\rho}_2 = 0)\psi(\boldsymbol{\rho}_1 = 0, \boldsymbol{\rho}_2)|^2, \tag{6}$$

where $\boldsymbol{\rho}_1 \equiv (x_1, y_1)$ and $\boldsymbol{\rho}_2 \equiv (x_2, y_2)$ are the transverse position vectors of the first and the second photon, then the position cross-spectral density function $W(\boldsymbol{\rho}_1, -\boldsymbol{\rho}_1)$ of the first photon is proportional to its conditional position probability distribution function $P(\boldsymbol{\rho}_1|\boldsymbol{\rho}_2 = 0)$, that is,

$$W(\boldsymbol{\rho}_1, -\boldsymbol{\rho}_1) \propto P(\boldsymbol{\rho}_1|\boldsymbol{\rho}_2 = 0). \tag{7}$$

Thus, by measuring the standard deviation of $W(\boldsymbol{\rho}_1, -\boldsymbol{\rho}_1)$, one can obtain the standard deviation of $P(\boldsymbol{\rho}_1|\boldsymbol{\rho}_2 = 0)$. We denote the standard deviation of the conditional x-position of the first photon by $\Delta(x_1|x_2 = 0)$. We note that although the above analysis has been presented with respect to making measurements on the first photon, we obtain the same result even when analysed with the second photon. Now, it is known that if the two-photon wavefunction is separable then the product U of the conditional uncertainties satisfies the Heisenberg uncertainty relation, that is,

$$U \equiv \Delta(x_1|x_2 = 0)\Delta(p_{1x}|p_{2x} = 0) \geqslant 0.5\hbar. \tag{8}$$

However, a violation of this inequality implies that the two-photon wavefunction is non-separable and that the two photons are entangled having EPR correlations in position–momentum variables [1].

SPDC is a nonlinear optical process in which a pump photon at higher frequency gets down-converted into two photons of lower frequencies called the signal and idler photons. In this process, a spatially perfectly coherent (pure) pump field gets down-converted into a spatially pure two-photon state [5, 8, 9, 11, 22, 35, 38–42]. Most of the SPDC experiments [4, 5, 7–11] utilize perfectly coherent Gaussian pump fields for generating a spatially pure two-photon state. For a Gaussian pump with beam waist at the crystal plane, the two-photon wavefunction produced by SPDC in the momentum basis is given by [8, 9, 22, 39]

$$\psi(\boldsymbol{p}_s, \boldsymbol{p}_i) = A \exp\left[-\frac{|\boldsymbol{p}_i + \boldsymbol{p}_s|^2\sigma_p^2}{4\hbar^2}\right] \exp\left[-\frac{|\boldsymbol{p}_i - \boldsymbol{p}_s|^2\sigma_-^2}{4\hbar^2}\right], \tag{9}$$

where $\boldsymbol{p}_s \equiv (p_{xs}, p_{ys})$ and $\boldsymbol{p}_i \equiv (p_{xi}, p_{yi})$ are the transverse momenta at the crystal plane of the signal and idler photons, respectively. In the above equation, A is a normalization constant, σ_p is the pump beam waist and $\sigma_- = \sqrt{0.455L\lambda_p/2\pi}$, where L is the length of the crystal, and λ_p is the pump wavelength. By taking the Fourier transform of the wavefunction given in equation (9), we write the two-photon wavefunction in the position basis as

$$\psi(\boldsymbol{\rho}_s, \boldsymbol{\rho}_i) = A' \exp\left[-\frac{|\boldsymbol{\rho}_i + \boldsymbol{\rho}_s|^2}{4\sigma_p^2}\right] \exp\left[-\frac{|\boldsymbol{\rho}_i - \boldsymbol{\rho}_s|^2}{4\sigma_-^2}\right]. \tag{10}$$

Here, A' is a normalization constant, $\boldsymbol{\rho}_s \equiv (x_s, y_s)$ and $\boldsymbol{\rho}_i \equiv (x_i, y_i)$ are the transverse position vectors of the signal and idler photons at the crystal plane. We note that the above wavefunctions $\psi(\boldsymbol{p}_s, \boldsymbol{p}_i)$ and $\psi(\boldsymbol{\rho}_s, \boldsymbol{\rho}_i)$ satisfy the conditions given in equations (4) and (6), respectively. The above functional forms of the wavefunctions have been widely used for studying spatial entanglement [8, 9, 22, 39]. We next experimentally demonstrate our proposed measurement technique for the two-photon state generated by SPDC.

3. Experiment and results

We present our experimental results demonstrating how the conditional position and momentum uncertainties can be obtained by measuring the cross-spectral density functions of just the signal photon. Figure 1(a) shows the schematic of the experimental setup for measuring position cross-spectral density function of the signal photon. An ultraviolet (UV) Gaussian pump beam of wavelength $\lambda_p = 405$ nm and beam waist $\sigma_p = 388$ μm is incident on a 2 mm thick $\beta-$barium borate crystal and produces two-photon state using SPDC with the type-I collinear phase-matching. We use a dichroic mirror (DM) to block the residual UV pump. We note that our experiment uses a spatially perfectly coherent pump field and involves no additional randomness. As a result, we expect that the experimentally generated two-photon state is pure in the spatial degree of freedom. The interferometer shown in figure 1(a) is used for measuring the cross-spectral density function of the signal photon field [33, 43]. Using this interferometer, we measure the

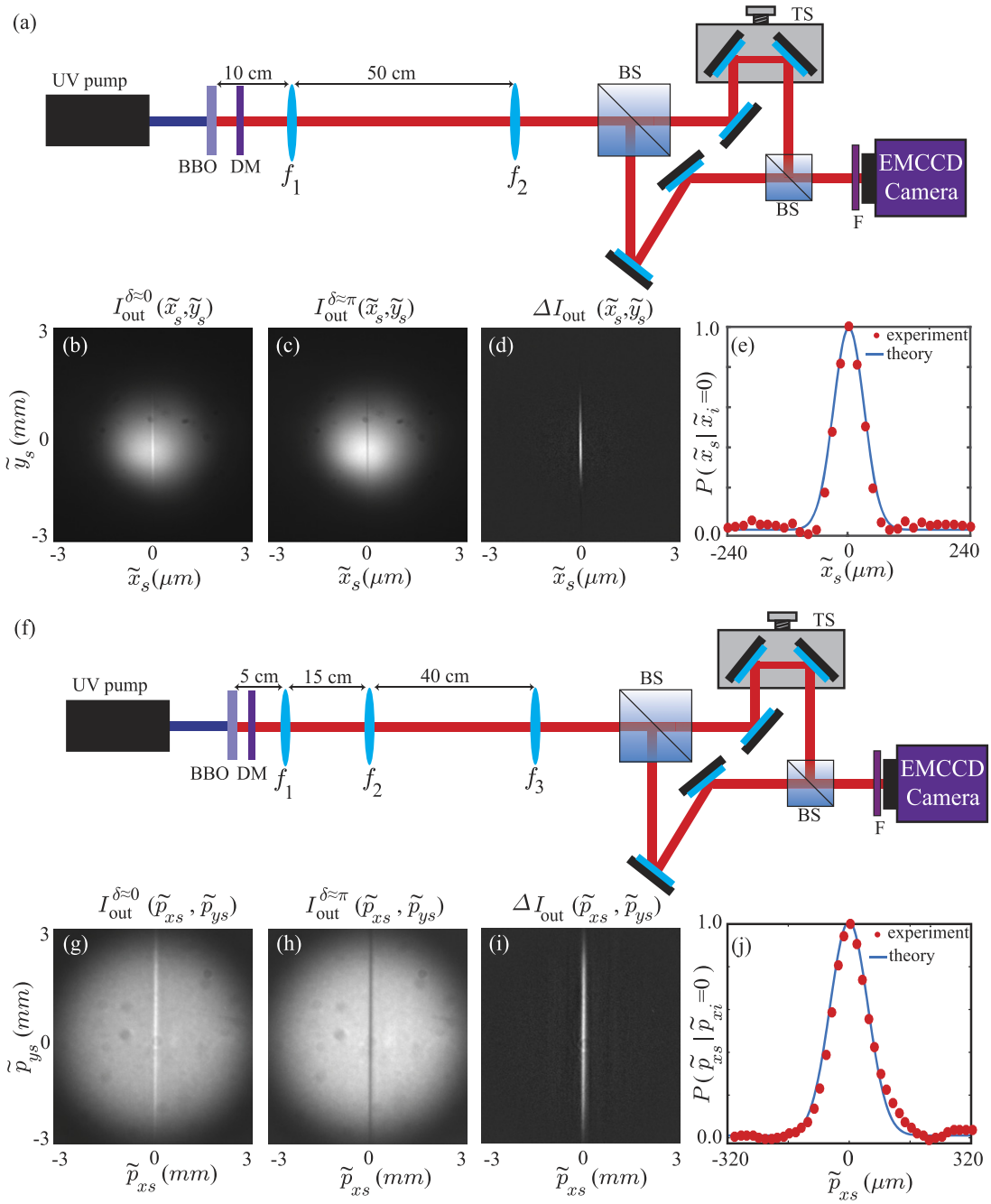

Figure 1. (a) Schematic of the experimental setup for measuring position cross-spectral density function. (b) and (c) The two interferograms recorded at $\delta_c = 0$ and $\delta_d = \pi$ with the configuration in figure (a). (d) The difference intensity image $\Delta I(\tilde{x}_s, \tilde{y}_s)$. (e) Experimental and theoretical conditional probability distribution $P(\tilde{x}_s|\tilde{x}_i = 0)$. (f) Schematic of the experimental setup for measuring momentum cross-spectral density function. (g) and (h) The two interferograms recoded at $\delta_c \approx 0$ and $\delta_d \approx \pi$ with the configuration in figure (f). (i) The difference intensity image $\Delta I(\tilde{p}_{xs}, \tilde{p}_{ys})$. (j) Experimental and theoretical conditional probability distribution $P(\tilde{p}_{xs}|\tilde{p}_{xi} = 0)$. DM: dichroic mirror, BS: beam splitter, TS: translational stage, F: an interference filter of 10 nm spectral width centred at 810 nm.

cross-spectral density at the crystal plane and use a 4-*f* configuration with $f_1 = 10$ cm and $f_2 = 40$ cm to image the crystal onto the EMCCD camera plane, kept at 40 cm from f_2, with a magnification $M = 4$. The EMCCD camera has 512×512 pixels with each pixel having an area of $16 \times 16\ \mu m^2$. We know that in collinear phase-matching, both signal and idler fields co-propagate and thus the intensity distribution recorded by the EMCCD camera becomes equal to the sum of the intensity distributions produced by the signal and idler fields. Furthermore, the signal and idler photon fields are identical in their spatial degree of freedom resulting in identical transverse intensity distributions. Therefore, the intensity distribution recorded by the EMCCD is same as that of the intensity distribution produced by either the signal or the idler photon field. In our experiments, the acquisition time of the EMCCD camera is kept at 60 s.

We take (x_s, y_s) and $(\tilde{x}_s, \tilde{y}_s)$ to be the position coordinates at the crystal plane and at the EMCCD plane, respectively. The two sets of coordinates are related as $\tilde{x}_s = Mx_s$ and $\tilde{y}_s = My_s$. The interferometer shown in figure 1(a) uses the wavefront inversion technique to measure cross-spectral density function and the details of this interferometer is presented in references [33, 43]. The intensity $I^{\delta}_{\text{out}}(\tilde{x}_s, \tilde{y}_s)$ of the output interferogram at the EMCCD plane is given by $I^{\delta}_{\text{out}}(\tilde{x}_s, \tilde{y}_s) = k_1 I(\tilde{x}_s, \tilde{y}_s) + k_2 I(-\tilde{x}_s, \tilde{y}_s) + 2\sqrt{k_1 k_2} W(\tilde{x}_s, \tilde{y}_s, -\tilde{x}_s, \tilde{y}_s) \cos\delta$ [33]. Here, k_1 and k_2 are the scaling constants, while $k_1 I(\tilde{x}_s, \tilde{y}_s)$ and $k_2 I(-\tilde{x}_s, \tilde{y}_s)$ are the intensities at the EMCCD plane coming through the two arms of the interferometer. The quantity δ is the phase difference between the two interferometric arms. We note that the functional form of above cross-spectral density function is real since it is proportional to conditional probability distribution function. If we take two interferograms $I^{\delta_c}_{\text{out}}(\tilde{x}_s, \tilde{y}_s)$ and $I^{\delta_d}_{\text{out}}(\tilde{x}_s, \tilde{y}_s)$ at $\delta = \delta_c$ and $\delta = \delta_d$, respectively, then it can be shown that the difference intensity $\Delta I_{\text{out}}(\tilde{x}_s, \tilde{y}_s) = I^{\delta_c}_{\text{out}}(\tilde{x}_s, \tilde{y}_s) - I^{\delta_d}_{\text{out}}(\tilde{x}_s, \tilde{y}_s)$ is proportional to the position cross-spectral density, that is, $\Delta I_{\text{out}}(\tilde{x}_s, \tilde{y}_s) \propto W(\tilde{x}_s, \tilde{y}_s, -\tilde{x}_s, \tilde{y}_s)$ [33, 43]. Figures 1(b) and (c) show the two experimentally measured interferograms at $\delta = \delta_c \approx 0$ and $\delta = \delta_d \approx \pi$, respectively, and figure 1(d) shows the difference intensity $\Delta I_{\text{out}}(\tilde{x}_s, \tilde{y}_s)$. From equation (7), we have that $W(\tilde{x}_s, \tilde{y}_s, -\tilde{x}_s, -\tilde{y}_s)$ is proportional to the conditional position probability distribution function of the signal photon, that is, $P(\tilde{x}_s, \tilde{y}_s | \tilde{x}_i = 0, \tilde{y}_i = 0) \propto W(\tilde{x}_s, \tilde{y}_s, -\tilde{x}_s, -\tilde{y}_s)$. Therefore, we obtain the one-dimensional conditional position probability distribution function $P(\tilde{x}_s | \tilde{x}_i = 0)$ by averaging $\Delta I_{\text{out}}(\tilde{x}_s, \tilde{y}_s)$ over the $\tilde{y}_s$-direction and plotting it in figure 1(e). Using equation (10) and the relevant experimental parameters, we calculate the theoretical $P(\tilde{x}_s | \tilde{x}_i = 0)$ and plot it in figure 1(e) (solid curve). We scale the $P(\tilde{x}_s | \tilde{x}_i = 0)$ plots in figure 1(e) such that the maximum value is one. We fit the experimental $P(\tilde{x}_s | \tilde{x}_i = 0)$ with a Gaussian function and find the standard deviation to be 26.25 μm. The standard deviation of the theoretical plot is 30.6 μm. Now, we use $\tilde{x}_s = Mx_s$ and obtain the experimental and theoretical values of $\Delta(x_s | x_i = 0)$ to be 6.56 μm and 7.65 μm, respectively.

Figure 1(f) shows the schematic of the experimental setup for measuring momentum cross-spectral density function of the signal photon. Here we measure the cross-spectral density function at the Fourier plane of the crystal by using the above mentioned wavefront inversion interferometric technique. We use the lens configuration with $f_1 = 5$ cm, $f_2 = 10$ cm, and $f_3 = 30$ cm for imaging the Fourier plane of the crystal on to the EMCCD camera. The EMCCD is kept at 30 cm from f_3. The effective focal length of this combination is $f_e = 15$ cm. The rest of the experimental parameters remain same as those in the above case of measuring the position cross-spectral density function. We take (p_{xs}, p_{ys}) to be the transverse momentum at the crystal plane and $(\tilde{p}_{xs}, \tilde{p}_{ys})$ to be the position coordinate at the EMCCD plane. These coordinates can be shown to be related as $p_{xs} = \frac{k_0 \hbar}{f_e} \tilde{p}_{xs}$ and $p_{ys} = \frac{k_0 \hbar}{f_e} \tilde{p}_{ys}$ [9], where $k_0 = \frac{2\pi}{\lambda_0}$. The intensity $I^{\delta}_{\text{out}}(\tilde{p}_{xs}, \tilde{p}_{ys})$ of the output interferogram at the EMCCD plane in this case can be written as $I^{\delta}_{\text{out}}(\tilde{p}_{xs}, \tilde{p}_{ys}) = k_1 I(\tilde{p}_{xs}, \tilde{p}_{ys}) + k_2 I(-\tilde{p}_{xs}, \tilde{p}_{ys}) + 2\sqrt{k_1 k_2} W(\tilde{p}_{xs}, \tilde{p}_{ys}, -\tilde{p}_{xs}, \tilde{p}_{ys}) \cos\delta$ [33]. Here, $k_1 I(\tilde{p}_{xs}, \tilde{p}_{ys})$, and $k_2 I(-\tilde{p}_{xs}, \tilde{p}_{ys})$ are the intensities at the EMCCD plane coming through the two interferometric arms. Just as discussed above, the difference intensity $\Delta I_{\text{out}}(\tilde{p}_{xs}, \tilde{p}_{ys}) = I^{\delta_c}_{\text{out}}(\tilde{p}_{xs}, \tilde{p}_{ys}) - I^{\delta_d}_{\text{out}}(\tilde{p}_{xs}, \tilde{p}_{ys})$ is proportional to the cross-spectral density function $W(\tilde{p}_{xs}, \tilde{p}_{ys}, -\tilde{p}_{xs}, \tilde{p}_{ys})$ [33, 43]. We record two interferograms at $\delta = \delta_c \approx 0$ and $\delta = \delta_d \approx \pi$. Figures 1(g) and (h) show the two experimentally measured interferograms at $\delta = \delta_c \approx 0$ and $\delta = \delta_d \approx \pi$, respectively, and figure 1(i) shows the difference intensity $\Delta I_{\text{out}}(\tilde{p}_{xs}, \tilde{p}_{ys})$. From equation (6), we have that $P(\tilde{p}_{xs}, \tilde{p}_{ys} | \tilde{p}_{xi} = 0, \tilde{p}_{yi} = 0) \propto W(\tilde{p}_{xs}, \tilde{p}_{ys}, -\tilde{p}_{xs}, -\tilde{p}_{ys})$. Therefore, we obtain the one-dimensional conditional probability distribution function $P(\tilde{p}_{xs} | \tilde{p}_{xi} = 0)$ by averaging $\Delta I_{\text{out}}(\tilde{p}_{xs}, \tilde{p}_{ys})$ over $\tilde{p}_{ys}$-direction and plotting it in figure 1(j). Using equation (9) and the relevant experimental parameters, we calculate the theoretical $P(\tilde{p}_{xs} | \tilde{p}_{xi} = 0)$ at the EMCCD plane and plot it in figure 1(j) (solid curve). We scale the $P(\tilde{p}_{xs} | \tilde{p}_{xi} = 0)$ plots in figure 1(j) such that the maximum value is one. We fit the experimental $P(\tilde{p}_{xs} | \tilde{p}_{xi} = 0)$ with a Gaussian function and find the standard deviation to be 49.5 μm. The standard deviation of the theoretical plot is 49.8 μm. Using $p_{xs} = \frac{k_0 \hbar}{f_e} \tilde{p}_{xs}$, we obtain the experimental and theoretical values of $\Delta(p_{xs} | p_{xi} = 0)$ to be $2.55 \times 10^{-3} \hbar\ \mu\text{m}^{-1}$ and $2.57 \times 10^{-3} \hbar\ \mu\text{m}^{-1}$, respectively.

As defined in equation (8), the experimentally measured value of the conditional uncertainty product U_{ex} is $1.67 \times 10^{-2} \hbar$. This is much smaller than $0.5\hbar$ and thus implies strong EPR correlations between the two entangled photons. We find the theoretical conditional uncertainty product U_{th} to be $1.96 \times 10^{-2} \hbar$, and we thus find a good match between the theory and experiments. Now, in order to quantify the accuracy of our experiment, we use the quantity $\mathcal{F} \equiv \frac{|U_{\text{th}} - U_{\text{ex}}|}{U_{\text{th}}}$. We note that a smaller value of $\mathcal{F}$ implies better experimental accuracy of EPR correlation measurements. For our experimental results, we obtain $\mathcal{F} = 0.147$. This value of $\mathcal{F}$ obtained through our measurement scheme is much smaller than the previously reported values of 0.270 in reference [11], 0.437 in reference [9], 0.660 in reference [5], 1.900 in reference [22], and 3.760 in reference [8]. We next focus on another quantity that is quite often used for quantifying the EPR-correlations measurements. It is called the degree of violation and is defined as $\mathcal{D} = \left(0.5\hbar / U_{\text{exp}}\right)^2$. The degree of violation $\mathcal{D}$ does not quantify the measurement accuracy but gives an

estimate of the degree with which the Heisenberg bound of $0.5\hbar$ is violated. For our experimental measurements, $\mathcal{D} = 896$, whereas the degree of violations reported earlier include 576 in reference [11], 380 in reference [9], 42 in reference [22], 25 in reference [5], and 4 in reference [8]. Thus we report not only the most accurate EPR-correlations measurements but also the highest degree of violation. This is because our intensity based measurement technique does not suffer from the issues such as too much loss, noise, long data collection time, and intensive post-processing, which are involved in coincidence based measurement techniques [8, 9, 11, 22].

4. Suitability of the technique for mixed two-photon states

So far we have demonstrated that our technique measures EPR correlations with very good accuracy for pure two-photon states that satisfy the conditions given in equations (4) and (6). Next, we numerically analyse the suitability of our technique for mixed two-photon states. In the case of mixed two-photon states, the widths of $W(x_s, -x_s)$ and $W(p_{xs}, -p_{xs})$ are not necessarily equal to $\Delta(x_s|x_i = 0)$ and $\Delta(p_{xs}|p_{xi} = 0)$ respectively. Suppose the widths of $W(x_s, -x_s)$ and $W(p_{xs}, -p_{xs})$ are μ_x and μ_{p_x}, respectively. Then the error $\mathcal{E}$ inherent in the scheme can be quantified as

$$\mathcal{E} \equiv \frac{|U_{\text{th}} - \mu_x \mu_{p_x}|}{U_{\text{th}}} \times 100\%, \tag{11}$$

where $U_{\text{th}} = \Delta(x_s|x_i = 0)\Delta(p_{xs}|p_{xi} = 0)$. The quantity $\mathcal{E}$ varies from 0 to 100%, and the higher values of $\mathcal{E}$ implies higher inaccuracies of the scheme for the mixed two-photon states.

There are two broad schemes by which one can generate mixed two-photon states. One is by introducing turbulence in the path of the generated pure two-photon state and the other one is by generating the two-photon states using a spatially partially coherent pump field. Next, for these two schemes of generating the mixed two-photon states, we numerically analyse how the inherent error $\mathcal{E}$ of our scheme changes as a function of the mixedness of the two-photon state.

4.1. Introducing mixedness through turbulence

We consider the situation in which both signal and idler photons pass through a planar turbulence medium right after the crystal plane. The turbulence introduces statistical randomness in both signal and idler photon fields. As a result, the two-photon state produced by SPDC does not remain pure and thus does not satisfy the conditions in equations (4) and (6). We write the mixed two-photon state thus produced using the two-photon cross-spectral density function in the position basis as

$$W_{\text{tp}}(\boldsymbol{\rho}_{s_1}, \boldsymbol{\rho}_{i_1}, \boldsymbol{\rho}_{s_2}, \boldsymbol{\rho}_{i2}) = \psi^*(\boldsymbol{\rho}_{s_1}, \boldsymbol{\rho}_{i_1})\psi(\boldsymbol{\rho}_{s_2}, \boldsymbol{\rho}_{i_2})W_{\text{turb}}(\boldsymbol{\rho}_{s_1}, \boldsymbol{\rho}_{s_2}, \boldsymbol{\rho}_{i_1}, \boldsymbol{\rho}_{i_2}), \tag{12}$$

where $\psi^*(\boldsymbol{\rho}_{s_1}, \boldsymbol{\rho}_{i_1})\psi(\boldsymbol{\rho}_{s_2}, \boldsymbol{\rho}_{i_2})$ is the two-photon cross-spectral density function just before the turbulence, and the influence of turbulence is captured by the cross-spectral density function $W_{\text{turb}}(\boldsymbol{\rho}_{s_1}, \boldsymbol{\rho}_{s_2}, \boldsymbol{\rho}_{i_1}, \boldsymbol{\rho}_{i_2}) = \exp\left[-6.88[|\boldsymbol{\rho}_{s_2} - \boldsymbol{\rho}_{s_1}|^2 + |\boldsymbol{\rho}_{i_2} - \boldsymbol{\rho}_{i_1}|^2]/(2r_0^2)\right]$ [44, 45], where r_0 is the so-called fried parameter. Smaller values of r_0 implies higher turbulence strength, with $r_0 = 0$ implying infinite turbulence and a completely mixed state and $r_0 = \infty$ implying no turbulence and thus a pure two-photon state.

From the above two-photon cross-spectral density function $W_{\text{tp}}(\boldsymbol{\rho}_{s_1}, \boldsymbol{\rho}_{s_2}, \boldsymbol{\rho}_{i_1}, \boldsymbol{\rho}_{i_2})$, we numerically calculate the one-dimensional conditional probability $P(x_s|x_i = 0)$ and the cross-spectral density function $W(x_s, -x_s)$ and evaluate their respective widths, $\Delta(x_s|x_i = 0)$ and μ_x, as a function of r_0 (see section 1.1 in supplementary material for details (https://stacks.iop.org/NJP/24/053033/mmedia).) We next find the corresponding two-photon momentum cross-spectral density function $W_{\text{tp}}(\boldsymbol{p}_{s_1}, \boldsymbol{p}_{i_1}, \boldsymbol{p}_{s_2}, \boldsymbol{p}_{i_2})$ using the following equation

$$W_{\text{tp}}(\boldsymbol{p}_{s_1}, \boldsymbol{p}_{i_1}, \boldsymbol{p}_{s_2}, \boldsymbol{p}_{i_2}) = \iiiint W_{\text{tp}}(\boldsymbol{\rho}_{s_1}, \boldsymbol{\rho}_{i_1}, \boldsymbol{\rho}_{s_2}, \boldsymbol{\rho}_{i_2}) e^{-i(\boldsymbol{\rho}_{s_1}\cdot\boldsymbol{p}_{s_1} + \boldsymbol{\rho}_{i_1}\cdot\boldsymbol{p}_{i_1} - \boldsymbol{\rho}_{s_2}\cdot\boldsymbol{p}_{s_2} - \boldsymbol{\rho}_{s_2}\cdot\boldsymbol{p}_{s_2})/\hbar} \times d\boldsymbol{\rho}_{s_1}\, d\boldsymbol{\rho}_{s_2}\, d\boldsymbol{\rho}_{i_1}\, d\boldsymbol{\rho}_{i_2}. \tag{13}$$

We then calculate the one-dimensional conditional momentum probability distribution function $P(p_{xs}|p_{xi} = 0)$ and the cross-spectral density function $W(p_{xs}, -p_{xs})$ of the signal photon and thereby the widths $\Delta(p_{xs}|p_{xi} = 0)$ and μ_{p_x} at different r_0 (see section 1.1 in supplementary material for details). Finally, we evaluate $\mathcal{E}$ as a function of r_0 and plot it in figure 2(a). We find that $\mathcal{E}$ decreases with increasing r_0. In other words, $\mathcal{E}$ decreases with decreasing turbulence strength. We note that the realistic turbulence is distributed and that the Fried parameter for realistic turbulences typically varies from $r_0 = 4$ mm to 30 mm

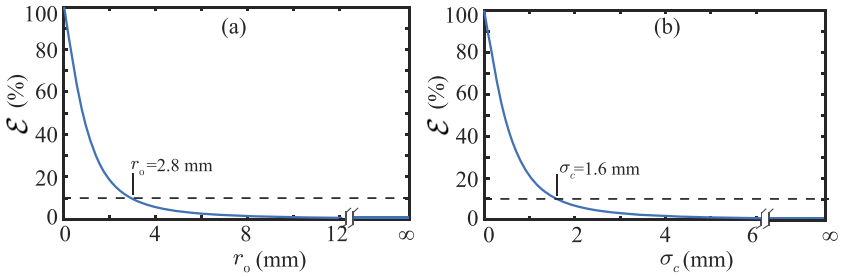

Figure 2. (a) Plot of error $\mathcal{E}$ as a function of the Fried parameter r_0 and (b) plot of error $\mathcal{E}$ as a function of the transverse coherence length σ_c of the pump field.

[46, 47]. We expect our results to remain valid even for a distributed turbulence, and from figure 2(a), we note that in the range from $r_0 = 4$ mm to 30 mm, the error $\mathcal{E}$ is less than 10%. We thus expect our technique to be practically useful even for measuring the EPR correlations of mixed two-photon state and thus be useful for experimental scenarios related to propagation of entangled photons through random media [45].

4.2. Introducing mixedness by using a spatially partially coherent pump field

Next, we consider the situation in which the two-photon states is produced by SPDC using a spatially partially coherent pump field. As a model of the spatially partially coherent field, we consider a Gaussian Schell model (GSM) field [48]. The generated mixed two-photon state can thus be described in terms of the following two-photon cross-spectral density function [49]:

$$W_{\rm tp}(\boldsymbol{\rho}_{s_1}, \boldsymbol{\rho}_{i_1}, \boldsymbol{\rho}_{s_2}, \boldsymbol{\rho}_{i_2}) = A \exp\left[-\frac{|\boldsymbol{\rho}_{s_1} + \boldsymbol{\rho}_{i_1}|^2 + |\boldsymbol{\rho}_{s_2} + \boldsymbol{\rho}_{i_2}|^2}{4\sigma_+^2}\right] \times \exp\left[-\frac{|\boldsymbol{\rho}_{s_2} + \boldsymbol{\rho}_{i_2} - \boldsymbol{\rho}_{s_1} - \boldsymbol{\rho}_{i_1}|^2}{2\sigma_c^2}\right] \exp\left[-\frac{|\boldsymbol{\rho}_{s_1} - \boldsymbol{\rho}_{i_1}|^2 + |\boldsymbol{\rho}_{s_2} - \boldsymbol{\rho}_{i_2}|^2}{4\sigma_-^2}\right], \quad (14)$$

where σ_+ is the beam-waist of the pump field at the crystal plane and σ_c is the transverse spatial coherence length of the pump at the crystal plane. The quantity σ_c ranges from 0 to ∞, with $\sigma_c = 0$ implying a completely mixed state and $\sigma_c = \infty$ implying a pure state. Using equation (14), we numerically calculate the one-dimensional conditional probability distribution $P(x_s|x_i = 0)$ and the cross-spectral density function $W(x_s, -x_s)$ as a function of σ_c (see section 1.2 in supplementary material for details). Next, using equation (14), we calculate two-photon momentum cross-spectral density function $W_{\rm tp}(\boldsymbol{p}_{s_1}, \boldsymbol{p}_{i_1}, \boldsymbol{p}_{s_2}, \boldsymbol{p}_{i_2})$ and thereby evaluate $P(p_{xs}|p_{xi} = 0)$ and $W(p_{xs}, -p_{xs})$ as a function of σ_c (see section 1.2 in supplementary material for details). Finally, using equation (11), we evaluate $\mathcal{E}$ and plot it as a function of σ_c in figure 2(b). We find that the error $\mathcal{E}$ decreases with increasing σ_c, that is, the error decreases as the purity of the two-photon state increases. From figure 2(b), we find that even with $\sigma_c = 1.6$ mm, which indicates substantial partial coherence, the error $\mathcal{E}$ is less than 10%. This implies that our scheme could be useful even for mixed two-photon states and thus be relevant for experimental scenarios involving spatially entangled mixed two-photon states [6, 50].

4.3. Measurement error as a function of mixedness in the two-photon state

Figures 2(a) and (b) show how the two common sources of mixedness affect the inherent error $\mathcal{E}$ of our scheme. Nevertheless, for conceptual clarity, we numerically calculate the inherent error as a function of the intrinsic degree of coherence P of the state in order to directly illustrate how $\mathcal{E}$ scales with the mixedness of the state. P is also known as a measure of the purity of the state [51–53]. It ranges from 0 to 1, with $P = 0$ implying a completely mixed state and $P = 1$ implying a pure state. We take $Q = 1 - P$ as a measure of the mixedness of the state and numerically analyse how the error $\mathcal{E}$ changes as a function of the mixedness Q. We take a two-photon mixed state produced using a GSM pump field. The two-photon cross-spectral density function of the field is given in equation (14). The mixedness of the state increases as the transverse coherence length σ_c of the GSM pump field is decreased. We quantify the mixedness of the two-photon state through $Q = 1 - P$, where $P = \sqrt{\int |W_{\rm tp}(\boldsymbol{\rho}_{s_1}, \boldsymbol{\rho}_{i_1}, \boldsymbol{\rho}_{s_2}, \boldsymbol{\rho}_{i_2})|^2 {\rm d}\boldsymbol{\rho}_{s_1}\, {\rm d}\boldsymbol{\rho}_{s_2}\, {\rm d}\boldsymbol{\rho}_{i_1}\, {\rm d}\boldsymbol{\rho}_{i_2}} = 1/\sqrt{1 + 4\sigma_+^2/\sigma_c^2}$ [51–53]. We calculate the error $\mathcal{E}$ inherent in the scheme as a function of the mixedness of the two-photon state and plot it in figure 3. We find that $\mathcal{E}$ scales only linearly with Q. We note that when a perfectly coherent Gaussian field is used as the pump, SPDC produces nearly pure two-photon states [4, 5, 7–11]. Nonetheless, from our above analysis, we find that even when the two-photon is state is not pure, the

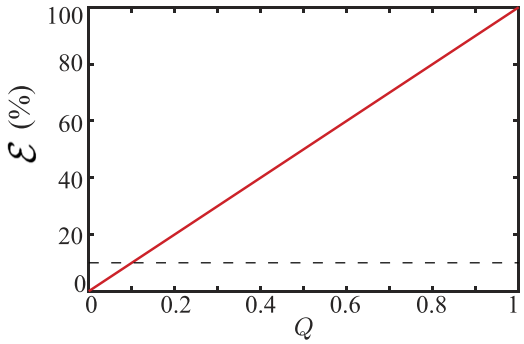

Figure 3. Plot of error $\mathcal{E}$ as a function of the mixedness Q.

inherent error scales only linearly. This means that even if the two-photon state has 5% mixedness, the error introduced by the scheme is only 5%. Thus our scheme could be useful even for mixed two-photon states and be thereby relevant for experimental scenarios that involve spatially entangled mixed two-photon states [6, 50].

5. Practical implications

We note that several quantum information applications require either the knowledge or measurement of position and momentum conditional probability distribution functions. For example, the resolution of a coincidence imaging scheme relies on conditional position and momentum uncertainties [25] and the communication protocols based on position–momentum entanglement require the measurement of conditional position and momentum probability distribution functions [21, 22]. Thus from the application perspective, it is important to have a technique that measures the EPR correlation accurately. So far, many coincidence imaging and communication protocols [22, 25–28, 54] have utilized the position–momentum entanglement of the two-photon state described by equations (9) and (10). Hence our measurement technique has direct applications in the above imaging and communication protocols. Moreover, we note that two-photon wavefunctions produced by non-collinear SPDC [40, 55], type-II SPDC [56], and spontaneous four-wave mixing [57, 58] processes satisfy the set of conditions given in equations (4) and (6). Thus our technique is applicable for certifying position–momentum entanglement in a range of processes. In this article, although we have demonstrated our scheme for the position–momentum EPR correlations, it could potentially be extended for measuring EPR-correlations in other continuous variables such as time-energy [12–14] and angle-OAM [15].

6. Conclusion

In conclusion, we have demonstrated a scheme for measuring two-photon position–momentum EPR correlations that does not require coincidence detection. Our method works for any pure two-photon state, irrespective of whether the state is separable or entangled. We have experimentally demonstrated this technique with the pure two-photon state produced with collinear phase-matching and have obtained the most accurate measurement of position–momentum EPR correlations reported so far. We have also presented a numerical analysis to study the suitability of this technique for a broad range of mixed two-photon states that do not satisfy the requisite conditions. Therefore, we expect our work to have practical implications for a wide range of experimental configurations and processes employed in continuous-variable quantum information applications.

Acknowledgments

We thank Siddharth Ramachandran for useful discussions and acknowledge financial support through the research Grant No. DST/ICPS/QuST/Theme-1/2019 from the Department of Science and Technology, Government of India. NM acknowledges post-doctoral fellowship from Indian Institute of Technology Kanpur.

Data availability statement

The data that support the findings of this study are available upon reasonable request from the authors.

ORCID iDs

Abhinandan Bhattacharjee https://orcid.org/0000-0002-0646-2404
Nilakantha Meher https://orcid.org/0000-0002-5057-5350
Anand K Jha https://orcid.org/0000-0002-5186-6264

References

[1] Einstein A, Podolsky B and Rosen N 1935 *Phys. Rev.* **47** 777
[2] Bell J S 1964 *Physics* **1** 195
[3] Wootters W K 1998 *Phys. Rev. Lett.* **80** 2245
[4] D'Angelo M, Kim Y H, Kulik S P and Shih Y 2004 *Phys. Rev. Lett.* **92** 233601
[5] Howell J C, Bennink R S, Bentley S J and Boyd R 2004 *Phys. Rev. Lett.* **92** 210403
[6] Zhang W, Fickler R, Giese E, Chen L and Boyd R W 2019 *Opt. Express* **27** 20745–53
[7] O'Sullivan-Hale M N, Khan I A, Boyd R W and Howell J C 2005 *Phys. Rev. Lett.* **94** 220501
[8] Leach J, Warburton R E, Ireland D G, Izdebski F, Barnett S, Yao A, Buller G S and Padgett M 2012 *Phys. Rev.* A **85** 013827
[9] Edgar M P, Tasca D S, Izdebski F, Warburton R E, Leach J, Agnew M, Buller G S, Boyd R W and Padgett M J 2012 *Nat. Commun.* **3** 984
[10] Reichert M, Defienne H and Fleischer J W 2018 *Sci. Rep.* **8** 7925
[11] Moreau P A, Devaux F and Lantz E 2014 *Phys. Rev. Lett.* **113** 160401
[12] Khan I A and Howell J C 2006 *Phys. Rev.* A **73** 031801
[13] MacLean J P W, Donohue J M and Resch K J 2018 *Phys. Rev. Lett.* **120** 053601
[14] Mei Y, Zhou Y, Zhang S, Li J, Liao K, Yan H, Zhu S L and Du S 2020 *Phys. Rev. Lett.* **124** 010509
[15] Leach J *et al* 2010 *Science* **329** 662–5
[16] Chen L, Ma T, Qiu X, Zhang D, Zhang W and Boyd R W 2019 *Phys. Rev. Lett.* **123** 060403
[17] Ou Z, Pereira S F, Kimble H and Peng K 1992 *Phys. Rev. Lett.* **68** 3663
[18] Ockeloen-Korppi C, Damskägg E, Pirkkalainen J M, Asjad M, Clerk A, Massel F, Woolley M and Sillanpää M 2018 *Nature* **556** 478–82
[19] Fadel M, Zibold T, Décamps B and Treutlein P 2018 *Science* **360** 409–13
[20] Josse V, Dantan A, Bramati A, Pinard M and Giacobino E 2004 *Phys. Rev. Lett.* **92** 123601
[21] Almeida M, Walborn S and Ribeiro P S 2005 *Phys. Rev.* A **72** 022313
[22] Dixon P B, Howland G A, Schneeloch J and Howell J C 2012 *Phys. Rev. Lett.* **108** 143603
[23] Brida G, Genovese M and Berchera I R 2010 *Nat. Photon.* **4** 227
[24] Bennink R S, Bentley S J, Boyd R W and Howell J C 2004 *Phys. Rev. Lett.* **92** 033601
[25] Aspden R S, Tasca D S, Boyd R W and Padgett M J 2013 *New J. Phys.* **15** 073032
[26] Asban S, Dorfman K E and Mukamel S 2019 *Proc. Natl Acad. Sci. USA* **116** 11673–8
[27] Toninelli E, Moreau P A, Gregory T, Mihalyi A, Edgar M, Radwell N and Padgett M 2019 *Optica* **6** 347–53
[28] Defienne H, Ndagano B, Lyons A and Faccio D 2021 *Nat. Phys.* **17** 591–7
[29] Hill S and Wootters W K 1997 *Phys. Rev. Lett.* **78** 5022
[30] Walborn S, Ribeiro P S, Davidovich L, Mintert F and Buchleitner A 2006 *Nature* **440** 1022–4
[31] Cheng L Y, Yang G H, Guo Q, Wang H F and Zhang S 2016 *Sci. Rep.* **6** 19482
[32] Jha A K, Agarwal G S and Boyd R W 2011 *Phys. Rev.* A **84** 063847
[33] Kulkarni G, Sahu R, Magaña-Loaiza O S, Boyd R W and Jha A K 2017 *Nat. Commun.* **8** 1054
[34] Kulkarni G, Taneja L, Aarav S and Jha A K 2018 *Phys. Rev.* A **97** 063846
[35] Pires H D L, Monken C and Van Exter M 2009 *Phys. Rev.* A **80** 022307
[36] Hochrainer A, Lahiri M, Lapkiewicz R, Lemos G B and Zeilinger A 2017 *Proc. Natl Acad. Sci. USA* **114** 1508–11
[37] Dixon P B, Howland G, Malik M, Starling D J, Boyd R and Howell J C 2010 *Phys. Rev.* A **82** 023801
[38] Walborn S P, Monken C, Pádua S and Ribeiro P S 2010 *Phys. Rep.* **495** 87–139
[39] Schneeloch J and Howell J C 2016 *J. Opt.* **18** 053501
[40] Law C and Eberly J 2004 *Phys. Rev. Lett.* **92** 127903
[41] Strekalov D V, Kim Y H and Shih Y 1999 *Phys. Rev.* A **60** 2685
[42] Just F, Cavanna A, Chekhova M V and Leuchs G 2013 *New J. Phys.* **15** 083015
[43] Bhattacharjee A, Aarav S and Jha A K 2018 *Appl. Phys. Lett.* **113** 051102
[44] Avetisyan H and Monken C 2016 *Opt. Express* **24** 2318–35
[45] Phehlukwayo S P, Umuhire M L, Ismail Y, Joshi S and Petruccione F 2020 *Phys. Rev.* A **102** 033732
[46] Krenn M, Handsteiner J, Fink M, Fickler R, Ursin R, Malik M and Zeilinger A 2016 *Proc. Natl Acad. Sci. USA* **113** 13648–53
[47] Krenn M, Fickler R, Fink M, Handsteiner J, Malik M, Scheidl T, Ursin R and Zeilinger A 2014 *New J. Phys.* **16** 113028
[48] Mandel L and Wolf E 1995 *Optical Coherence and Quantum Optics* (Cambridge: Cambridge University Press)
[49] Jha A K and Boyd R W 2010 *Phys. Rev.* A **81** 013828
[50] Defienne H and Gigan S 2019 *Phys. Rev.* A **99** 053831
[51] Patoary A S M, Kulkarni G and Jha A K 2019 *J. Opt. Soc. Am.* B **36** 2765–76
[52] Meher N, Patoary A S M, Kulkarni G and Jha A K 2020 *J. Opt. Soc. Am.* B **37** 1224–30
[53] Hutter L, Lima G and Walborn S P 2020 *Phys. Rev. Lett.* **125** 193602
[54] Zhang L, Silberhorn C and Walmsley I A 2008 *Phys. Rev. Lett.* **100** 110504

[55] Van Exter M, Aiello A, Oemrawsingh S, Nienhuis G and Woerdman J 2006 *Phys. Rev.* A **74** 012309
[56] Srivastav V, Valencia N H, Leedumrongwatthanakun S, McCutcheon W and Malik M 2021 arXiv:2110.03462
[57] Lee J C, Park K K, Zhao T M and Kim Y H 2016 *Phys. Rev. Lett.* **117** 250501
[58] Zhang W, Dong M X, Ding D S, Shi S, Wang K, Liu S L, Zhou Z Y, Guo G C and Shi B S 2019 *Phys. Rev.* A **100** 012347